GEOPHYSICS, VOL. 77, NO. 3 (MAY-JUNE 2012); P. S65–S72, 7 FIGS.
10.1190/GEO2011-0460.1

Compensation for transmission losses based on one-way propagators in the mixed domain

Weijia Sun[1] and Li-Yun Fu[1]

ABSTRACT

Most true-amplitude migration algorithms based on one-way wave equations involve corrections of geometric spreading and seismic Q attenuation. However, few papers discuss the compensation of transmission losses (CTL) based on one-way wave equations. Here, we present a method to compensate for transmission losses using one-way wave propagators for a 2D case. The scheme is derived from the Lippmann-Schwinger integral equation. The CTL scheme is composed of a transmission term and a phase-shift term. The transmission term compensates amplitudes while the wave propagates through subsurfaces. The transmission term is a function of the vertical wavenumbers of two adjacent heterogeneous screens. The phase-shift term is a Fourier finite-difference (FFD) propagator implemented in a mixed domain via Fourier transform. The transmission term can be flexibly incorporated into the conventional phase-shift migration algorithm, i.e., FFD, at every depth step. We analyze the effects of frequency, lateral velocity contrast, and vertical velocity ratio on the accuracy of the presented formulae. Numerical examples from a flat model and a fault model with lateral velocity variations are presented to demonstrate the ability of the proposed scheme for compensation of transmission losses.

INTRODUCTION

Wavenumber-domain wavefield extrapolation based on the one-way wave equation (Claerbout, 1985) is a powerful tool for accurate imaging of reflectors in complex geologic structures. Although one-way wave equations can provide accurate kinematic information (e.g., phases), they cannot treat the dynamic information (e.g., amplitudes) well. Several factors, such as geometric spreading, seismic Q-attenuation, and transmission losses, can prevent one-way wave migration algorithms from producing true-amplitude.

Most current true-amplitude migration algorithms include only geometrical spreading (Zhang et al., 2003, 2005; Vivas and Pestana, 2010), and Q-compensation based on one-way wave-equation migration has been discussed by many authors (Dai and West, 1994; Mittet et al., 1995; Valenciano et al., 2011; Wang, 2008; Yu et al., 2002), but transmission losses during migration have been paid little attention. Deng and McMechan (2007) presented a two-pass recursive algorithm to compensate for transmission losses using the framework of full-wave prestack reverse time migration (RTM) (Chang and McMechan, 1986). However, the method is challenged by huge computational cost mainly from the two-pass RTM: the first pass extracts information required for the compensation, and the second pass applies the compensation for each major reflector. Luo et al. (2005) use the transmission coefficient and WKBJ approximation to correct the localized one-way beamlet propagators. Although some authors (Xu et al., 1998; Zhang et al., 2003) tried to compensate for transmission losses using post or prestack migration, compensation for transmission losses (CTL) has not yet been sufficiently accurate (Deng and McMechan, 2007). In other applications, Massier et al. (1997) estimate transmission operators for a subsurface region to remove shallow reverberations. Frijlink and Wapenaar (2004) derive a correction method for transmission losses based on energy-conservation principles and the power reciprocity theorem for acoustic media. Based on energy-conservation principles, Angus (2007) present amplitude corrections for the problem of transmission losses using a narrow-angle one-way elastic wave equation. However, the problem of transmission losses still has not been treated properly for one-way wave propagators.

Here, we first derived one-way propagators coupled with transmission coefficients starting from the Lippmann-Schwinger integral equation. Generally, conventional one-way propagators without the CTL consider amplitude behavior only for one interface boundary at depth z, making it difficult for these methods to fully account for

Manuscript received by the Editor 18 November 2011; revised manuscript received 4 January 2012; published online 22 March 2012.
[1]Institute of Geology and Geophysics, Key Laboratory of Petroleum Resource Research, Chinese Academy of Sciences, Beijing, China. E-mail: swj@mail.iggcas.ac.cn; lfu@mail.iggcas.ac.cn.

transmission losses. The proposed method in this paper considers transmission losses for a given slab with two screens. The first screen is the same as in conventional methods at depth z, and the second screen is immediately below the first one at depth $z + \Delta z$, allowing us to treat transmission phenomena naturally. The compensation scheme in this paper is composed of a compensation term (transmission coefficient) multiplied by a Fourier finite-difference (FFD) one-way wave propagator (Ristow and Rühl, 1994). The transmission coefficient is a function of the vertical wavenumbers of two adjacent heterogeneous screens, and the proposed scheme is perfectly suited to the FFD method. The transmission compensation is performed during the prestack depth migration in a natural way, which makes the compensation flexible and efficient. Comparing with the theoretical transmission coefficient, we examine the computational accuracy of our method for several cases, involving frequency, lateral velocity contrast, and vertical velocity ratio, and frequency dependence. Numerical results from a flat model and a fault model with lateral velocity variations suggest that the scheme behaves well for these cases.

THEORY

For one-way wave equations, a medium can be sliced into heterogeneous slabs (see Figure 1) perpendicular to the preferred propagation direction along the vertical z-axis. A heterogeneous slab is defined by Ω with the top interface Γ_1 at depth z_1, the bottom interface Γ_2 at depth z_2, and thickness $\Delta z = z_2 - z_1$. The velocity distribution in the slab is denoted by $v(\mathbf{r})$, where $\mathbf{r}$ is the positional vector. We assume the wave propagates along the z-axis, crossing the slab from the upper boundary Γ_1 to the lower boundary Γ_2.

We start with the scalar Helmholtz equation for a time-harmonic wavefield $u(\mathbf{r})$ in a constant-density medium

$$\nabla^2 u(\mathbf{r}) + k^2 u(\mathbf{r}) = 0, \tag{1}$$

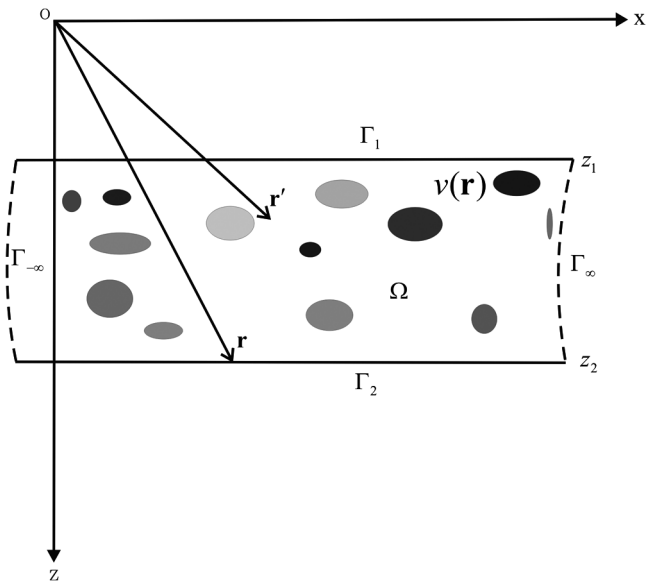

Figure 1. The geometry of a heterogeneous slab. The slab Ω is bounded by the top boundary Γ_1 at depth z_1, the bottom boundary Γ_2 at depth z_2, the left boundary $\Gamma_{-\infty}$ and the right boundary Γ_∞. The point $\mathbf{r}$ is the observation point, while $\mathbf{r}'$ denotes the scattering point.

where the wavenumber $k = \omega/v(\mathbf{r})$, and $\mathbf{r} = (x, z)$ represents the observation point located at the boundary Γ_2 of any given slab. Note that we neglect the source term, which can be considered as the initial condition. The total pressure wavefield $u(\mathbf{r})$ at location $\mathbf{r} \in \Omega$ is composed of two scattered fields

$$u(\mathbf{r}) = u_1^s(\mathbf{r}) + u_2^s(\mathbf{r}). \tag{2}$$

The scattered field $u_1^s(\mathbf{r})$ is attributable to the closed boundary structure, $\Gamma = \Gamma_1 + \Gamma_2 + \Gamma_{-\infty} + \Gamma_\infty$, and satisfies the boundary integral equation

$$u_1^s(\mathbf{r}) = \int_\Gamma \left[G(\mathbf{r}, \mathbf{r}') \frac{\partial u(\mathbf{r}')}{\partial n} - u(\mathbf{r}') \frac{\partial G(\mathbf{r}, \mathbf{r}')}{\partial n} \right] d\mathbf{r}', \tag{3}$$

where $\partial/\partial n$ denotes differentiation with respect to the outward normal of the boundary Γ. The scattered field $u_2^s(\mathbf{r})$ is arising from the volume heterogeneities within the slab and satisfies the Lipmann-Schwinger integral equation

$$u_2^s(\mathbf{r}) = k_0^2 \int_\Omega O(\mathbf{r}') u(\mathbf{r}') G(\mathbf{r}, \mathbf{r}') d\mathbf{r}', \tag{4}$$

where $k_0 = \omega/v_0$ is the reference wavenumber associated with a chosen reference velocity v_0, $O(\mathbf{r}) = n^2(\mathbf{r}) - 1$ is the relative slowness perturbation with acoustic refractive index $n(\mathbf{r}) = v_0/v(\mathbf{r})$, and $\mathbf{r}' = (x', z')$ denotes the scattering point locating at the boundary Γ_1 in equation 3 and in the volume of the slab in equation 4.

These Kirchhoff-Helmholtz integral representation formulas are derived using the Green's function $G(\mathbf{r}, \mathbf{r}')$ in the background medium; that is, $G(\mathbf{r}, \mathbf{r}') = iH_0^{(1)}(k_0|\mathbf{r} - \mathbf{r}'|)/4$ for 2D problems, where the complex unit $i = \sqrt{-1}$ and $H_0^{(1)}$ is the Hankel function of the first kind and of zeroth order. Substituting equations 3 and 4 into equation 2, we obtain the following generalized Lippmann-Schwinger integral equation

$$\begin{aligned} &\int_\Gamma \left[G(\mathbf{r}, \mathbf{r}') \frac{\partial u(\mathbf{r}')}{\partial n} - u(\mathbf{r}') \frac{\partial G(\mathbf{r}, \mathbf{r}')}{\partial n} \right] d\mathbf{r}' \\ &\quad + k_0^2 \int_\Omega O(\mathbf{r}') u(\mathbf{r}') G(\mathbf{r}, \mathbf{r}') d\mathbf{r}' \\ &\quad = \begin{cases} u(\mathbf{r}) & \mathbf{r} \in \Omega \\ C(\mathbf{r}) u(\mathbf{r}) & \mathbf{r} \in \Gamma \\ 0 & \mathbf{r} \notin \bar{\Omega} \end{cases}, \end{aligned} \tag{5}$$

for all $\mathbf{r}' \in \bar{\Omega} = \Omega + \Gamma$, where the coefficient $C(\mathbf{r}) = 1/2$ for a flat Γ. Equation 5 is a wave integral equation that is equivalent to the Helmholtz equation 1 and describes the two-way wave propagations in a heterogeneous medium (Fu, 2003).

The closed boundary Γ is composed of the top boundary Γ_1, the bottom boundary Γ_2, the left boundary $\Gamma_{-\infty}$, and the right boundary Γ_∞. Thus, the right-hand side of equation 3 can be rewritten as

$$\int_{\Gamma}\left[G(\mathbf{r},\mathbf{r}\prime)\frac{\partial u(\mathbf{r}\prime)}{\partial n}-u(\mathbf{r}\prime)\frac{\partial G(\mathbf{r},\mathbf{r}\prime)}{\partial n}\right]d\mathbf{r}\prime$$
$$=\int_{\Gamma_1+\Gamma_2}\left[G(\mathbf{r},\mathbf{r}\prime)\frac{\partial u(\mathbf{r}\prime)}{\partial n}-u(\mathbf{r}\prime)\frac{\partial G(\mathbf{r},\mathbf{r}\prime)}{\partial n}\right]d\mathbf{r}\prime$$
$$+\int_{\Gamma_{-\infty}}\left[G(\mathbf{r},\mathbf{r}\prime)\frac{\partial u(\mathbf{r}\prime)}{\partial n}-u(\mathbf{r}\prime)\frac{\partial G(\mathbf{r},\mathbf{r}\prime)}{\partial n}\right]d\mathbf{r}\prime$$
$$+\int_{\Gamma_{\infty}}\left[G(\mathbf{r},\mathbf{r}\prime)\frac{\partial u(\mathbf{r}\prime)}{\partial n}-u(\mathbf{r}\prime)\frac{\partial G(\mathbf{r},\mathbf{r}\prime)}{\partial n}\right]d\mathbf{r}\prime. \quad (6)$$

For convenience, let $q(\mathbf{r})=\partial u(\mathbf{r})/\partial n$ indicate the acoustic pressure gradient. For 2D problems, the plane-wave representation of the Hankel function in a homogeneous medium is given by

$$H_0^{(1)}(k_0|\mathbf{r}-\mathbf{r}\prime|)=\frac{1}{\pi}\int_{-\infty}^{\infty}k_{z1}^{-1}\exp[ik_{z1}(z-z\prime)+ik_x(x-x\prime)]dk_x$$
$$=\frac{1}{\pi}\int_{-\infty}^{\infty}k_{z1}^{-1}\exp(ik_{z1}\Delta z)\exp(-ik_xx\prime)\exp(ik_xx)dk_x, \quad (7)$$

where k_{z1} is the vertical wavenumber at boundary Γ_1, and Δz is the thickness of the slab. Applying equation 7 to the integrands in equation 6, we obtain

$$\int_{\Gamma_1}\left[G(\mathbf{r},\mathbf{r}\prime)\frac{\partial u(\mathbf{r}\prime)}{\partial n}-u(\mathbf{r}\prime)\frac{\partial G(\mathbf{r},\mathbf{r}\prime)}{\partial n}\right]d\mathbf{r}\prime$$
$$=\frac{1}{4\pi}\int_{-\infty}^{\infty}\left[ik_{z1}^{-1}q(k_x,z_1)+u(k_x,z_1)\right]\exp(ik_{z1}\Delta z)\exp(ik_xx)dk_x \quad (8)$$

and

$$\int_{\Gamma_2}\left[G(\mathbf{r},\mathbf{r}\prime)\frac{\partial u(\mathbf{r}\prime)}{\partial n}-u(\mathbf{r}\prime)\frac{\partial G(\mathbf{r},\mathbf{r}\prime)}{\partial n}\right]d\mathbf{r}\prime$$
$$=\frac{1}{4\pi}\int_{-\infty}^{\infty}ik_{z1}^{-1}q(k_x,z_2)\exp(ik_xx)dk_x. \quad (9)$$

Because the boundaries $\Gamma_{-\infty}$ and Γ_{∞} tend to $\pm\infty$ along the x-axis direction, the slab Ω becomes unbounded and extends infinitely along the x-axis direction. In this case, the Sommerfeld boundary condition will be automatically satisfied because of the integral representation of radiating solutions. Thus, the boundary integrals on $\Gamma_{-\infty}$ and Γ_{∞} become zero, given by

$$\int_{\Gamma_{-\infty}}\left[G(\mathbf{r},\mathbf{r}\prime)\frac{\partial u(\mathbf{r}\prime)}{\partial n}-u(\mathbf{r}\prime)\frac{\partial G(\mathbf{r},\mathbf{r}\prime)}{\partial n}\right]d\mathbf{r}\prime\to 0, \quad (10)$$

and

$$\int_{\Gamma_{\infty}}\left[G(\mathbf{r},\mathbf{r}\prime)\frac{\partial u(\mathbf{r}\prime)}{\partial n}-u(\mathbf{r}\prime)\frac{\partial G(\mathbf{r},\mathbf{r}\prime)}{\partial n}\right]d\mathbf{r}\prime\to 0. \quad (11)$$

Substituting equation 7 into the volume integral term in equation 5, and using the rectangle rule to calculate the integration over z (i.e., $\int_a^b f(z)dz\approx f(a)(b-a)$), we have

$$k_0^2\int_{\Omega}O(\mathbf{r}\prime)u(\mathbf{r}\prime)G(\mathbf{r},\mathbf{r}\prime)d\mathbf{r}\prime$$
$$=\frac{k_0}{4\pi}\int_{-\infty}^{\infty}k_{z1}^{-1}[F(k_x,z_1)\exp(ik_{z1}\Delta z)]\exp(ik_xx)dk_x, \quad (12)$$

where $F(k_x,z_1)$ represents the Fourier transform of the velocity-weighted wavefield $F(\mathbf{r})=ik_0\Delta zO(\mathbf{r})u(\mathbf{r})$. For detailed derivation of equations 8, 9, and 12, please see appendix A. Equation 12 is actually the Born approximation applied to the slab. It requires that the slab be thin enough with respect to the wavelength of incident waves to avoid large numerical errors while applying the rectangle rule. Substituting equations 8, 9, 10, 11, and 12 into equation 5 and noting that each inner integral in equation 8, 9, and 12 is a Fourier transform, we obtain a wavenumber-domain wave equation

$$k_{z1}u(k_x,z_2)-iq(k_x,z_2)=[k_{z1}u(k_x,z_1)+iq(k_x,z_1)+k_0F(k_x,z_1)]\exp(ik_{z1}\Delta z). \quad (13)$$

Equation 13 describes the one-way wave propagation in a heterogeneous slab between Γ_1 and Γ_2.

In exploration geophysics, we measure the pressure wavefield $u(\mathbf{r})$, but not the pressure gradient $q(\mathbf{r})$. One possible way to drop the pressure gradient $q(\mathbf{r})$ at the slab entrance Γ_1 is to choose Γ_1 as an acoustically soft boundary (Dirichlet boundary condition). Dropping the pressure gradient $q(\mathbf{r})$ means multiple reflections and transmissions are neglected, which leads to a single scattering approximation. The other way is to build a boundary integral equation at the boundary Γ_1. Here, we build a boundary integral equation given by

$$\frac{1}{2}u(\mathbf{r})-\int_{\Gamma_1}\left[G(\mathbf{r},\mathbf{r}\prime)\frac{\partial u(\mathbf{r}\prime)}{\partial n}-u(\mathbf{r}\prime)\frac{\partial G(\mathbf{r},\mathbf{r}\prime)}{\partial n}\right]d\mathbf{r}\prime=0,\qquad \mathbf{r},\mathbf{r}'\in\Gamma_1. \quad (14)$$

Expressing equation 14 in the same way as equation 9, we have

$$iq(k_x,z_1)=k_{z1}u(k_x,z). \quad (15)$$

Substituting equation 15 into equation 13 leads to

$$k_{z1}u(k_x,z_2)-iq(k_x,z_2)=[2k_{z1}u(k_x,z)+k_0F(k_x,z)]\exp(ik_{z1}\Delta z). \quad (16)$$

To account for transmission loss at Γ_2 in a natural manner, we need to build a boundary integral equation at the bottom of the slab given by

$$\frac{1}{2}u(\mathbf{r})-\int_{\Gamma_2}\left[G(\mathbf{r},\mathbf{r}\prime)q(\mathbf{r}\prime)+u(\mathbf{r}\prime)\frac{\partial G(\mathbf{r},\mathbf{r}\prime)}{\partial n}\right]d\mathbf{r}\prime=0,\qquad \mathbf{r},\mathbf{r}\prime\in\Gamma_2. \quad (17)$$

Applying the plane-wave representation of the Hankel function to equation 17 results in

$$iq(k_x,z_2)=-k_{z2}u(k_x,z_2), \quad (18)$$

where k_{z2} is the wavenumber related to the medium immediately below Γ_2. Substituting equation 18 into equation 16 gives

$$u(k_x, z_2) = \frac{2k_{z1}}{k_{z1} + k_{z2}}[u(k_x, z_1) + \frac{k_0}{k_{z1}} F(k_x, z_1)] \exp(ik_{z1}\Delta z). \tag{19}$$

Equation 19 is a one-way downward propagator under the single-scattering approximation that accounts for the accumulated effect on wave amplitudes and phases of forward scattering by volume heterogeneities inside the slab and the transmissions between adjoining slabs.

Equation 19 can be written in a generalized form as

$$u(k_x, z + \Delta z) = T(k_{z1}, k_{z2}; z)\mathbf{E}[u(k_x, z)], \tag{20}$$

where

$$T(k_{z1}, k_{z2}) = \frac{2k_{z1}}{k_{z1} + k_{z2}}, \tag{21}$$

is the transmission coefficient at a given depth z, and the extrapolation operator

$$\mathbf{E}[u(k_x, z)] = [u(k_x, z_1) + \frac{k_0}{k_{z1}} F(k_x, z_1)] \exp(ik_{z1}\Delta z), \tag{22}$$

is the FFD propagator (Ristow and Rühl, 1994). The vertical wavenumbers k_{z1} and k_{z2}, dependent on the space vector $\mathbf{r}$, are calculated by equation 24 below. The implementation of $F(k_x, z_1)$ requires a deconvolution in the wavenumber domain. A regular way to implement $F(k_x, z_1)$ is to use the finite-difference method in the space domain, which is equivalent to the FFD method.

From equation 20, the proposed one-way propagator is composed of two terms: transmission-coefficient-compensating amplitudes, and conventional FFD propagator governing amplitudes and phases. Consequently, the algorithm structure might allow the compensation term (equation 21) to be incorporated into other phase-shift operators in the mixed domain, e.g., split-step Fourier method (Stoffa et al., 1990) for media with a weak lateral velocity contrast, a generalized screen propagator (de Hoop et al., 2000), or even amplitude-preserving one-way propagators (Zhang et al., 2005; Vivas and Pestana, 2010). However, this needs to be verified in the future, for it is not the focus of this paper.

The compensation scheme of equation 21 can be easily extended to 3D cases. For either 2D or 3D, transmission coefficient is a function of the two vertical wavenumbers k_{z1} and k_{z2} corresponding to two adjacent slabs at depths z_1 and z_2. The calculation of the vertical wavenumbers coincides with the algorithm structure of the conventional one-way method.

RELATIONSHIP WITH PREVIOUS WORK

Deng and McMechan (2007) explicitly presented a two-pass recursive algorithm to compensate for transmission losses. Because they implemented their scheme using a prestack RTM (Chang and McMechan, 1986), their method needed two steps to compensate for transmission losses. The first step is to obtain information required for the compensation, e.g., reflection coefficients obtained from a division of receiver and source wavefields, the incident angle, and the velocity ratio, all of which requires performing prestack RTM. The second pass is to compensate for transmission losses via performing the prestack RTM once more. Thus, their method was challenged by huge computational cost.

Applying the dispersion relationship $k_{z1} = \frac{\omega}{v_1} \cos\theta_1$ and $k_{z2} = \frac{\omega}{v_2} \cos\theta_2$ (Claerbout, 1985) to equation 21, we obtain the same formula as Deng and McMechan (2007):

$$T = \frac{2v_2 \cos\theta_1}{v_2 \cos\theta_1 + v_1 \cos\theta_2} = \frac{2v_2/v_1 \cos\theta_1}{v_2/v_1 \cos\theta_1 + \cos\theta_2}, \tag{23}$$

where θ and v denote the propagation angle and velocity of the media, and subscripts 1 and 2 mean the two adjoining heterogeneous screens. Thus, the transmission coefficient calculated by our scheme in the wavenumber domain is equivalent to the theoretical one. The calculation, however, may suffer numerical errors resulted from the numerical implementation of two vertical wavenumbers corresponding to two adjacent screens at depth z_1 and z_2.

IMPLEMENTATION

The compensation scheme can be easily incorporated into conventional phase-shift modeling or migration algorithms. Three steps are required to implement the FFD: (1) a phase shift in the wavenumber domain, (2) a phase correction in the space domain, and (3) a finite-difference correction in the space domain. The CTL term can be applied after the first step of implementing the FFD.

Because a slab involves upper and lower screens at depths z_1 and z_2, only one reference velocity is employed during wavefield extrapolation. This is different from the regular way. To make the FFD algorithm stable, we choose the minimum velocity as the reference velocity. The approximate cascaded vertical wavenumber for the FFD propagator can be expressed as

$$k_z(\mathbf{r}) = k_{z0} + \omega\left(\frac{1}{v(\mathbf{r})} - \frac{1}{v_0}\right) - \frac{bk_x^2}{1 - ak_x^2}, \tag{24}$$

for 2D cases, where $k_{z0} = \sqrt{\omega^2/v_0^2 - k_x^2}$, ω is the angular frequency, $a = 0.25(v_0^2 + v_0 v + v^2)/\omega^2$ and $b = 0.5(v - v_0)/\omega$. The horizontal wavenumber k_x is discretized as $k_x = i2\pi/(N_x dx)$, $i = 1, 2, \cdots, N_x$, N_x is the sampling number, and dx is the sampling interval in the x-direction.

Because the circular frequency ω cannot be removed directly, the compensation term (equation 21) is dependent on frequency. The calculation of the vertical wavenumber involves the lateral velocity contrast. The accuracy of the transmission term (see equation 23) is also related to the vertical velocity ratio of the two adjacent slabs. Thus, we would evaluate the influences of the frequency, the lateral velocity contrast, and the vertical velocity ratio of media, on the accuracy of our method in the next section.

EXAMPLES

In this section, we investigate the dependence of accuracy of the presented scheme on frequency, lateral velocity contrast and vertical velocity ratio. To obtain valid values for parameters, e.g., velocity contrast, we extract these parameters from the SEG/EAGE 2D salt model. The thickness of a slab is 12.192 m.

Here, the lateral velocity contrast is defined as $p = v_0/v$, where v_0 is the reference velocity, and v is the migration velocity in a heterogeneous slab. The vertical velocity ratio is defined as $r = v_1/v_2$, where v_1 and v_2 are the reference velocities of the two adjoining

slabs. The velocity contrast p ranges from 0.3 to 1, while the velocity ratio r ranges from 0.8 to 1.2 approximately for the SEG/EAGE 2D salt model.

Dependence on frequency

The presented scheme is dependent on the frequency, while the theoretical coefficients are not frequency-dependent. Thus, it is necessary to examine the frequency characteristics of the transmission coefficients calculated by equation 21. We first set $v_1 = 2200$ m/s. Reference velocities for the SEG/EAGE 2D salt model range from 2000 m/s to 2400 m/s. In this example, we have $p = 1$ and $r = 0.8$.

Figure 2 compares the calculated transmission coefficients for two frequencies, 5 Hz and 20 Hz, compared with the theoretical coefficients at different frequencies. We investigated frequencies of $f = 5$ Hz, 20 Hz. We also computed the transmission coefficients for the frequencies of $f = 50$ Hz, 80 Hz, and 100 Hz, and found that the coefficients calculated with a frequency larger than 20 Hz are the same as those calculated with a 20 Hz frequency. The frequency-dependent transmission coefficient is consistent with the theoretical ones for low- and high-frequency components at small and intermediate incident angles. However, a small numerical error arises at large incident angles (greater than 70°) for the low-frequency components.

Dependence on lateral velocity contrast

The SEG/EAGE 2D salt model shows a large lateral velocity contrast, ranging from 0.3 to 1. A small velocity contrast denotes a strong lateral velocity variation and a large one denotes a weak lateral velocity variation. To avoid the influence of frequency, we use a high frequency $f = 20$ Hz. Because the lateral velocity contrast in the model varies between 0.4 and 0.6 mostly, we choose $p = 0.4$, 0.6, and 0.8, denoting strong, intermediate, and weak lateral velocity contrasts, respectively.

Figure 3 shows comparisons of the calculated transmission coefficients with the theoretical ones for a velocity ratio 0.8. They coincide with each other for incident angles smaller than 50°; but for a large incident angle (greater than 50°), numerical errors become large. However, the errors disappear when $p = 1$, i.e., no lateral velocity contrast involved. This could result from the approximation of the vertical wavenumber (see Figure 4) for a different velocity contrast p for FFD propagator. In other words, the dispersion accuracy of propagators has effect on the accuracy of the transmission coefficients. However, the computational accuracy can be improved further by using other one-way propagators with higher accuracy, because they can provide more accurate information for dip angles larger than 50°.

Dependence on vertical velocity ratio

The vertical velocity ratio ranges from 0.8 to 1.2 for the SEG/EAGE 2D salt model. We take the case of a ratio smaller than 1one as an example. The ratio varies from 0.3 to 0.9, denoting large, intermediate, and small velocity contrast in the depth direction. We also take $p = 0.9$ and $f = 20$ Hz.

Figure 5 compares the coefficient calculated by equation 21 with the theoretical coefficients for different velocity ratios. As observed in above result, the present schemes behave well for small and

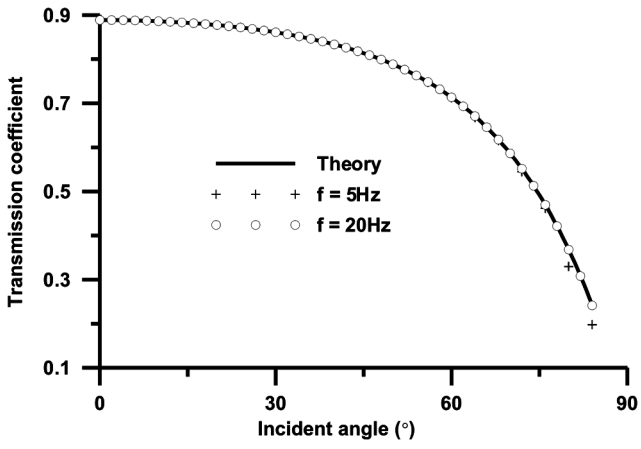

Figure 2. Comparison of the computed frequency-dependent transmission coefficient with the theoretical one for different frequencies. The lateral velocity contrast $p = 1$, and the velocity ratio is 0.8.

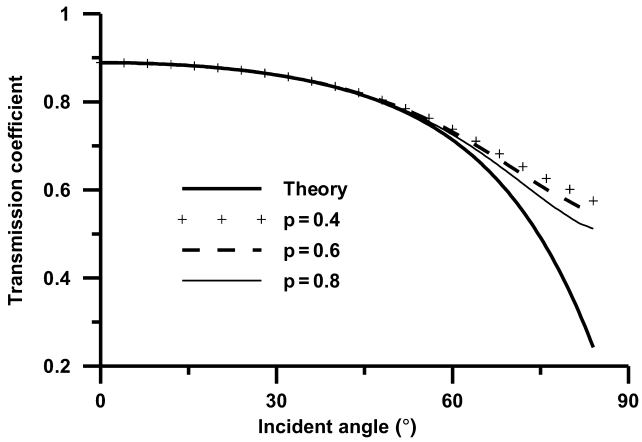

Figure 3. Comparison of the transmission coefficient calculated by equation 21 with the theoretical one for different lateral velocity contrasts. The frequency is 20 Hz, and the velocity ratio is 0.8.

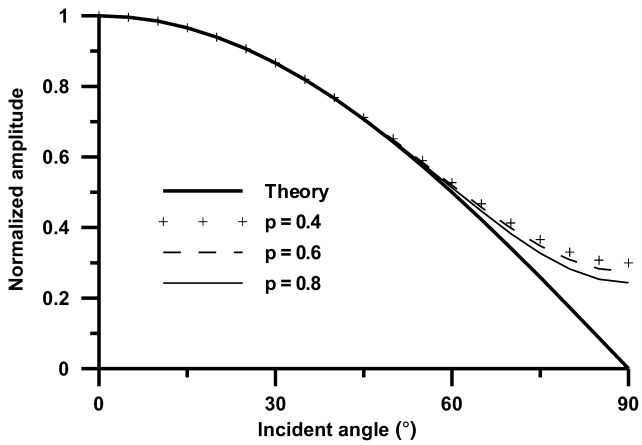

Figure 4. Comparison of the approximate vertical wavenumber for different velocity contrasts with the theoretical one.

intermediate incident angle (smaller than 50°). Large errors occur at large incident angles, which is resulted from the approximation of the vertical wavenumber.

Two simple models

We consider two simple models in a 2D medium: a horizontal two-layer model shown in Figure 6a and a two-layer fault model with lateral velocity variations shown in Figure 7a. Both models are defined on a grid system of 1001×201 with a grid spacing of 12 m × 5 m in the horizontal and vertical directions, respectively. The velocities of the upper and lower layers are 2250 m/s and 2000 m/s. We synthesize a shot record to examine the accuracy of our method. The source locates at the horizontal position 6 km. The peak frequency is 15 Hz, and the time sampling interval is 4 ms.

To eliminate other factors that affect the transmission across interfaces as much as possible, two receiver lines are placed above and below the subsurface to receive the incident waves and the transmitted waves, respectively. The transmission coefficient is defined by the ratio of amplitudes of the transmitted waves and the incident waves. The transmission coefficients calculated by our CTL method are compared with those by the full-wave finite-difference (FD) method and the one-way method without CTL. Because reflections occur while waves propagate through the interface using full-wave FD method, we pick the peak amplitudes of the first arrivals of incident waves and transmitted waves. We use the root-mean-square as the amplitudes of the incident waves and transmitted waves for the one-way method.

Figure 6b compares the transmission coefficient calculated by the one-way method with CTL (equation 21) with those calculated with the full-wave FD method and the one-way method without CTL (equation 22) for the flat model shown in Figure 6a. The shot is located at horizontal position 6 km. The calculated amplitudes by the one-way method without CTL show large errors compared with that calculated by the full-wave FD method. This illustrates that the conventional one-way method (Claerbout, 1985) cannot provide the correct dynamic information of waves. In contrast, the calculated amplitudes by our method match well with the results of the full-wave FD method.

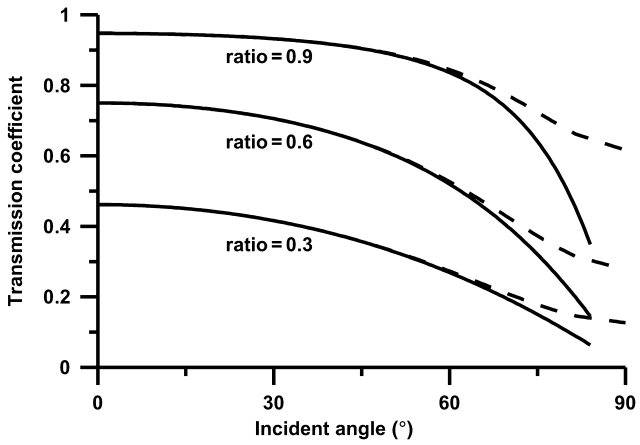

Figure 5. The transmission coefficients calculated with different vertical velocity ratios, i.e., 0.3, 0.6, and 0.9. The solid line denotes the theoretical transmission coefficient, while the dashed line denotes the transmission coefficient calculated by equation 21.

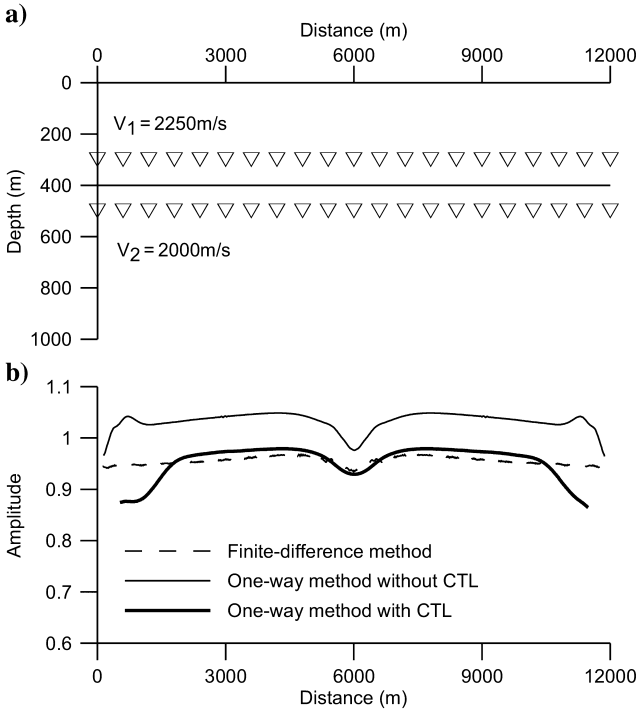

Figure 6. (a) A flat model with two layers. The triangles denote receivers above and below the interface. (b) Comparison of the amplitudes calculated by the one-way method with CTL (thick solid line) with the full-wave FD method (dash line) and the one-way method without CTL (thin solid line) for the flat model.

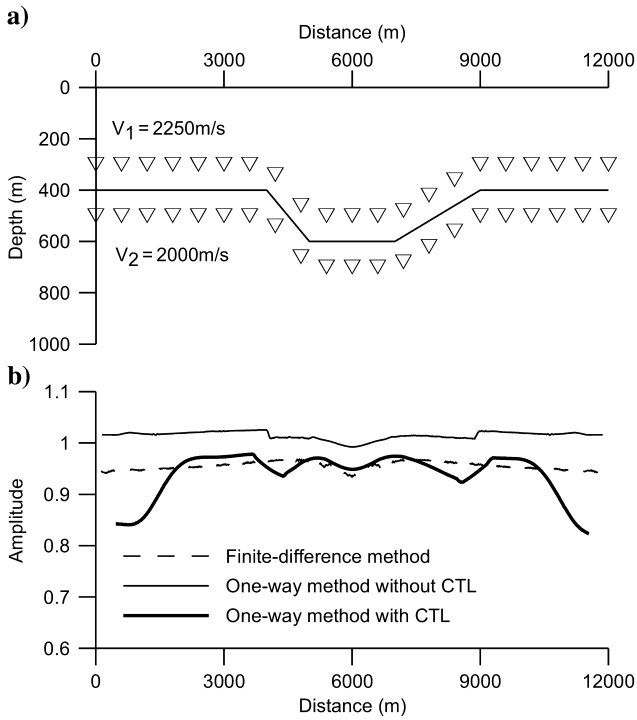

Figure 7. (a) A fault model with two layers. The triangles denote receivers above and below the interface. (b) Comparison of the amplitudes calculated by the one-way method with CTL (thick solid line) with the full-wave FD method (dash line) and the one-way method without CTL (thin solid line) for the fault model.

To show behavior of our correction method for a model of lateral velocity variation, we consider the fault model shown in Figure 7a. Figure 7b shows results of the one-way method with and without CTL and the full-wave FD method for a single shot located at horizontal position 6 km. As expected, the result by the conventional one-way method shows large amplitude errors compared with that of the full-wave FD method. Thus, the conventional one-way method does not treat the transmission losses properly. Our method has taken CTL into account, so its result behaves well in comparison with that of full-wave FD method. Approximately, 2% slight bias of the transmission coefficient curves of our method relative to those of the FD method occurs in Figures 6b and 7b, perhaps the result of geometry spreading or other approximations.

In Figures 6b and 7b, amplitudes with CTL decrease obviously when the distance is less than 2 km and more than 10 km approximately. This means the calculations of the transmission coefficients are inaccurate. The incident angle at 2 km or 10 km is about 85°. Thus, this does not affect the compensation scheme, because the phases of one-way propagators are also inaccurate when the propagation angle is beyond 85°.

CONCLUSIONS

We have presented a scheme to compensate for the transmission losses based on the one-way wave propagator in the mixed domain. The CTL scheme does not change the algorithm structure of the conventional one-way migration algorithm, and the compensation term can be flexibly incorporated into a FFD scheme. Compared with the theoretical solutions, the presented scheme behaves well in complex structures, e.g., strong lateral velocity contrast and steep dip (up to 50°). Numerical examples from a horizontally layered model and a fault model with lateral velocity variations show that the conventional one-way method does not provide reliable amplitudes as a result of transmission losses. Our method in contrast accounts for transmission losses correctly as shown in comparison with the result from the full-wave FD method. The proposed method can be extended to 3D cases easily, because the compensation term is a simple function of vertical wavenumbers of two screens at depths z_1 and z_2. The possibility of extending the formulas to other one-way phase-shift algorithms will be investigated in the future.

ACKNOWLEDGMENTS

We are grateful to associate editors, Ken Larner, Jan Thorbecke, and Binzhong Zhou for their valuable comments and corrections of the English expressions. Criticisms from one anonymous reviewer are also appreciated. This research is supported by the National Natural Science Foundation of China (Grant No. 41104079) and the China Postdoctoral Science Foundation (Grant No. 20100480447).

APPENDIX A

MATHEMATICAL DERIVATIONS

The Green's function in a 2D case is given by

$$G(\mathbf{r},\mathbf{r}\prime)=\frac{i}{4\pi}\int_{-\infty}^{\infty}k_{z1}^{-1}\,\exp(ik_{z1}\Delta z)\,\exp(-ik_x x')\,\exp(ik_x x)dk_x, \tag{A-1}$$

and its normal derivative can be expressed as

$$\frac{\partial G(\mathbf{r},\mathbf{r}\prime)}{\partial n}=-\frac{1}{4\pi}\int_{-\infty}^{\infty}\exp(ik_{z1}\Delta z)\exp(-ik_x x\prime)\exp(ik_x x)dk_x. \tag{A-2}$$

For the point $\mathbf{r}\prime$ located at the boundary Γ_1, the microelement $d\mathbf{r}\prime$ can be written as $dx\prime$. Thus, the boundary integral equation at Γ_1 becomes

$$\begin{aligned}\int_{\Gamma_1}\left[G(\mathbf{r},\mathbf{r}\prime)q(\mathbf{r}\prime)-u(\mathbf{r}\prime)\frac{\partial G(\mathbf{r},\mathbf{r}\prime)}{\partial n}\right]d\mathbf{r}\prime&=\frac{1}{4\pi}\int_{-\infty}^{\infty}ik_{z1}^{-1}\,\exp(ik_z\Delta z)\,\exp(ik_x x)\\&\int_{-\infty}^{\infty}q(x\prime,z_1)\exp(-ik_x x\prime)dx\prime dk_x\\&+\frac{1}{4\pi}\int_{-\infty}^{\infty}\exp(ik_{z1}\Delta z)\exp(ik_x x)\\&\int_{-\infty}^{\infty}u(x\prime,z_1)\exp(-ik_x x\prime)dx\prime dk_x\\&=\frac{1}{4\pi}\int_{-\infty}^{\infty}\left[ik_z^{-1}q(k_x,z_1)+u(k_x,z_1)\right]\\&\exp(ik_{z1}\Delta z)\exp(ik_x x)dk_x.\end{aligned} \tag{A-3}$$

Because $\frac{\partial G(\mathbf{r},\mathbf{r}\prime)}{\partial n}=\frac{\partial G(\mathbf{r},\mathbf{r}\prime)}{\partial z}\frac{\partial z}{\partial n}=0$ when $\mathbf{r}$ and $\mathbf{r}'\in\Gamma_2$, the boundary integral equation at Γ_2 becomes

$$\begin{aligned}\int_{\Gamma_2}\left[G(\mathbf{r},\mathbf{r}\prime)q(\mathbf{r}\prime)-u(\mathbf{r}\prime)\frac{\partial G(\mathbf{r},\mathbf{r}\prime)}{\partial n}\right]d\mathbf{r}\prime&=\frac{1}{4\pi}\int_{-\infty}^{\infty}ik_{z_1}^{-1}\,\exp(ik_{z_1}\Delta z)\exp(ik_x x)\\&\int_{-\infty}^{\infty}q(x\prime,z)\,\exp(-ik_x x\prime)dx\prime dk_x\\&=\frac{1}{4\pi}\int_{-\infty}^{\infty}ik_{z_1}^{-1}q(k_x,z_1)\,\exp(ik_{z_1}\Delta z)\exp(ik_x x)dk_x\\&=\frac{1}{4\pi}\int_{-\infty}^{\infty}ik_{z_1}^{-1}q(k_x,z_2)\,\exp(ik_x x)dk_x,\end{aligned} \tag{A-4}$$

where $q(k_x,z_2)\approx q(k_x,z_1)\exp(ik_{z_1}\Delta z)$. To calculate an integral over a function $f(x)$ on the interval (z_1,z_2) numerically, the rectangle rule is defined as

$$\int_{z_1}^{z_2}f(x)dx\approx f(z_1)(z_2-z_1). \tag{A-5}$$

The volume integration in equation 5 is given by

$$\begin{aligned}k_0^2\int_{\Omega}O(\mathbf{r}\prime)u(\mathbf{r}\prime)d\mathbf{r}\prime=\frac{k_0}{4\pi}\int_{x\prime}\frac{1}{i\Delta z}G(\mathbf{r},\mathbf{r}\prime)dx\prime\\\int_{z\prime}ik_0\Delta z O(\mathbf{r}\prime)u(\mathbf{r}\prime)dz\prime.\end{aligned} \tag{A-6}$$

Applying equation A-5 and substituting equations A-1 and A-2 into equation A-6, we obtain

$$k_0^2 \int_\Omega O(\mathbf{r}\prime)u(\mathbf{r}\prime)d\mathbf{r}\prime = k_0 \int_{x\prime} \frac{1}{i\Delta z} G(\mathbf{r}, \mathbf{r}\prime)F(\mathbf{r}\prime)\Delta z dx\prime$$
$$= \frac{k_0}{4\pi} \int_{-\infty}^{\infty} \exp(ik_{z1}\Delta z)\exp(ik_x x)$$
$$\int_{-\infty}^{\infty} F(x\prime, z_1)\exp(-ik_x x\prime)dx\prime dk_x$$
$$= \frac{k_0}{4\pi} \int_{-\infty}^{\infty} k_{z1}^{-1}[F(k_x, z_1)\exp(ik_{z1}\Delta z)]\exp(ik_x x)dk_x. \quad \text{(A-7)}$$

REFERENCES

Angus, D. A., 2007, True amplitude corrections for a narrow-angle one-way elastic wave equation: Geophysics, **72**, no. 2, T19–T26, doi: 10.1190/1.2430694.

Chang, W. F., and G. A. McMechan, 1986, Reverse-time migration of offset vertical seismic profiling data using the excitation-time imaging condition: Geophysics, **51**, 67–84, doi: 10.1190/1.1442041.

Claerbout, J. F., 1985, Imaging the earth's interior: Blackwell Scientific Publications, Inc..

Dai, N., and G. F. West, 1994, Inverse *Q* migration: 64th Annual International Meeting, SEG, Expanded Abstracts, 1418–1421.

de Hoop, M. V., J. H. L. Rousseau, and R.-S. Wu, 2000, Generalization of the phase-screen approximation for the scattering of acoustic waves: Wave Motion, **31**, 43–70, doi: 10.1016/S0165-2125(99)00026-8.

Deng, F., and G. A. McMechan, 2007, True-amplitude prestack depth migration: Geophysics, **72**, no. 3, S155–S166, doi: 10.1190/1.2714334.

Frijlink, M., and K. Wapenaar, 2004, Migration with correction for transmission losses in arbitrarily homogeneous media: 74th Annual International Meeting, SEG, Expanded Abstracts, 1029–1032.

Fu, L. Y., 2003, Numerical study of generalized Lipmann-Schwinger integral equation including surface topography: Geophysics, **68**, 665–671, doi: 10.1190/1.1567236.

Luo, M. Q., R. S. Wu, and X. B. Xie, 2005, True amplitude one-way propagators implemented with localized corrections on beamlets: 75th Annual International Meeting, SEG, Expanded Abstracts, 1966–1969.

Massier, M. R. F., G. C. Herman, and D. J. Verschuur, 1997, Removal of overburden transmission effects by deterministic deconvolution: Geophysics, **62**, 1612–1616, doi: 10.1190/1.1444263.

Mittet, R., R. Sollie, and K. Hokstad, 1995, Prestack depth migration with compensation for absorption and dispersion: Geophysics, **60**, 1485–1494, doi: 10.1190/1.1443882.

Ristow, D., and T. Ruhl, 1994, Fourier finite-difference migration: Geophysics, **59**, 1882–1893, doi: 10.1190/1.1443575.

Stoffa, P. L., J. T. Fokkema, R. M. d. L. Freire, and W. P. Kessinger, 1990, Split-step Fourier migration: Geophysics, **55**, 410–421, doi: 10.1190/1.1442850.

Valenciano, A. A., N. Chemingui, D. Whitmore, and S. Brandsberg-Dahl, 2011, Wave equation migration with attenuation and anisotropy compensation: 81st Annual International Meeting, SEG, Expanded Abstracts, 232–236.

Vivas, F. A., and R. C. Pestana, 2010, True-amplitude one-way wave equation migration in the mixed domain: Geophysics, **75**, no. 5, S199–S209, doi: 10.1190/1.3478574.

Wang, Y., 2008, Inverse-*Q* filtered migration: Geophysics, **73**, no. 1, S1–S6, doi: 10.1190/1.2806924.

Xu, T., H. Zhang, and G. A. McMechan, 1998, Amplitude compensation of seismic data: Application to masking by shallow bright spots: Journal of Seismic Exploration, **7**, 173–198.

Yu, Y., R. S. Lu, and M. M. Deal, 2002, Compensation for the effects of shallow gas attenuation with viscoacoustic wave-equation migration: 72nd Annual International Meeting, SEG, Expanded Abstracts, 2062–2065.

Zhang, Y., G. Zhang, and N. Bleistein, 2003, True amplitude wave equation migration arising from true amplitude one-way wave equations: Inverse Problems, **19**, 1113–1138, doi: 10.1088/0266-5611/19/5/307.

Zhang, Y., G. Zhang, and N. Bleistein, 2005, Theory of true-amplitude one-way wave equations and true-amplitude common-shot migration: Geophysics, **70**, no. 4, E1–E10, doi: 10.1190/1.1988182.